UNIVERSITY OF CALIFORNIA

SANTA CRUZ

HUMAN RHODOPSIN: A FRESH VIEW

A thesis submitted in partial satisfaction

of the requirements for the degree of

MASTER OF SCIENCE

in

CHEMISTRY

by

Owen Williams

September 2014

The Thesis of Owen Williams is approved:

_____

Professor David Kliger, Advisor

_____

Professor Ólöf Einarsdóttir, Chair

_____

Tyrus Miller

Vice Provost and Dean of Graduate Studies

_____

Professor Jin Zhang

Table of Contents:

List of Figures:

Abstract:

Human Rhodopsin: A Fresh View

Owen Williams

This work examines the microsecond and millisecond photochemistry of human rhodopsin. There have been significant advances in the mechanistic and structural understanding of bovine rhodopsin over the last two decades that have not been applied to human rhodopsin. This study uses time-resolved absorbance spectroscopy to probe human rhodopsin in its native disk membrane. Human rhodopsin is first studied at pH 7.0 and 20°C from 1 μs – 128 μs to explore the lumirhodopsin I – lumirhodopsin II equilibrium. The remainder of this work examines human rhodopsin at pH 8.7 and 15°C from 5 μs – 120 ms to study the activation mechanism from lumirhodopsin I to metarhodopsin II. The intermediates seen in the bovine rhodopsin mechanism are present in human rhodopsin, but with differing kinetics. The processes observed in human rhodopsin are slower than in bovine rhodopsin, and the equilibria are shifted towards 380 nm product compared to bovine rhodopsin under similar conditions.

Acknowledgements:

First of all, I would like to thank my advisor, Dave Kliger, for taking me into his lab and his guidance and support over the last few years. I have learned an incredible amount from him, not just about polarized light and biophysics, but about how to think like a scientist.

I also want to thank the members of the Kliger group. Particular thanks are due to Jim, who has a truly immense breadth and depth of knowledge. I really appreciated our conversations, both scientific and personal. Everything I know about SVD and data analysis came from Bob and Istvan. Eefei's wet lab experience and CD expertise were invaluable in getting my experiments off the ground. Chie's help with the data collection, particularly towards the end, was very welcome. In addition to the scientific help, everybody was very supportive and encouraging. I can't think of a better place to have worked the last three years.

A huge thank you goes to my family, without whose love and support I would have never made it this far. Even halfway across the country, you've always been there for me in good times and bad. Part of me will always be with you no matter where I go.

Finally, but certainly not least, thanks to Nicole for putting up with me throughout this entire process. You've been incredibly supportive and understanding, and you remind me of what's really important. I hope I can do the same for you when it's your turn for grad school, and I eagerly await the many more years we have ahead of us.

Chapter 1: Rhodopsin

1.1 Overview of vision

Vision begins when a photon strikes a photoreceptor. Humans have four photoreceptors: three cone pigments used in color vision, and rhodopsin, which is responsible for dim light vision. While all of these photoreceptors are important for vision, rhodopsin is considerably easier to isolate and study, so it makes a convenient model system for all of the photoreceptors. Rhodopsin is located in the disk membranes of rod photoreceptor cells (Figure 1). It features a covalently bound retinal chromophore, which is attached via a protonated Schiff base linkage to lysine 296. In its dark-adapted state, the retinal chromophore is in the 11-*cis* configuration. Rhodopsin photochemistry begins when a photon interacts with its retinal chromophore, isomerizing it from 11-*cis* to all-*trans*. This induces a conformational shift in rhodopsin, which results in helix VI moving to reveal a binding cleft for the G-protein transducin after a few milliseconds. Transducin then releases its bound GDP, triggering the signaling cascade that eventually leads to an action potential and neuron firing.

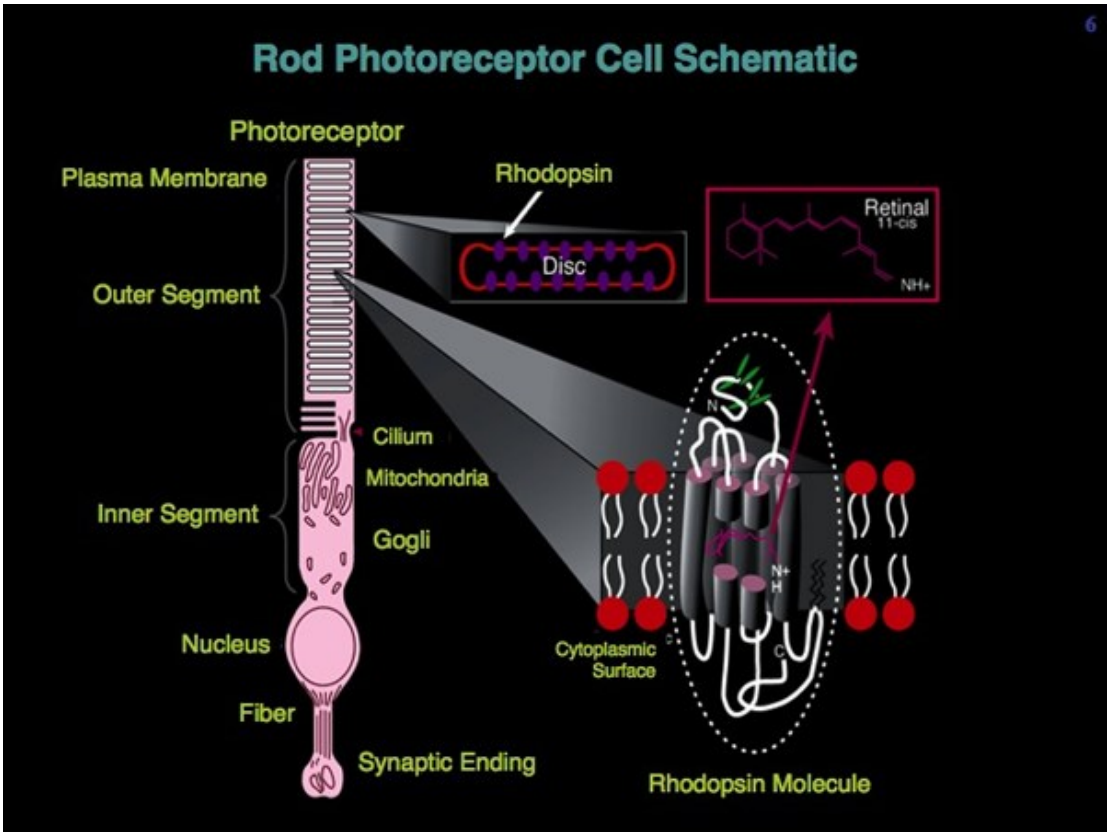

Figure 1: Diagram of a rod cell (from http://www.sakmarlab.org/WhatWeDo/VisionSensoryNeuroscience/Figure4.html)

1.2 Rhodopsin as a GPCR

In addition to its role in vision, rhodopsin is an excellent model of a G-protein coupled receptor (GPCR). GPCRs make up approximately 36% of drug targets (*1*), so there is quite a bit of interest in understanding how they are activated and repressed. Unlike most GPCRs, rhodopsin is uniquely accessible to fast time-resolved optical spectroscopy. Rhodopsin is not activated by binding to a signaling molecule, but by absorbing a photon. This allows precise temporal and spatial control of when rhodopsin is activated, enabling time resolution not possible with a

diffusion-controlled reaction. Furthermore, rhodopsin has absorption bands centered at 500 nm and 340 nm due to its retinal chromophore. These absorption bands are sensitive to the chromophore environment, so as rhodopsin shifts between its progressive intermediates, the chromophore environment changes, which produces a varying ultraviolet-visible absorption spectrum, which is easily detected with time-resolved absorption spectroscopy. The combination of optical excitation and probing enables the time-resolved study of rhodopsin at any desired time scale, which is not true for most other GPCRs. The insights gained from studying rhodopsin are invaluable for understanding the detailed mechanism of GPCR activation, as rhodopsin is uniquely accessible for sensitive optical investigation.

1.3 Bovine Rhodopsin

Rhodopsin has been studied in several animal species. While the human version is the most relevant for human health, human rhodopsin is difficult to obtain in large amounts since it cannot be extracted without destroying the retina. Bovine rhodopsin, however, can be obtained as a byproduct of the beef industry. Human and bovine rhodopsin share 93% sequence identity and many of the differing amino acids are located at the helix-membrane interface (*2*), so the functional and kinetic differences are expected to be relatively minor. Since bovine rhodopsin can be purified in 50-100 mg quantities in a single preparation, it is an attractive choice for extensive study.

1.3.1 Bovine Rhodopsin Structure

Rhodopsin is a class A GPCR with seven transmembrane helices. It consists of the apoprotein, opsin, and a retinal chromophore. A major advance in rhodopsin research occurred in 2000 when the first crystal structure of rhodopsin was published by Palczewski and coworkers (*3*). Since then, rhodopsin has been crystallized in a variety of forms, including in its active state (*4*). A structure from 2004 obtained by Schertler and colleagues is presented in Figure 2 below (*5*).

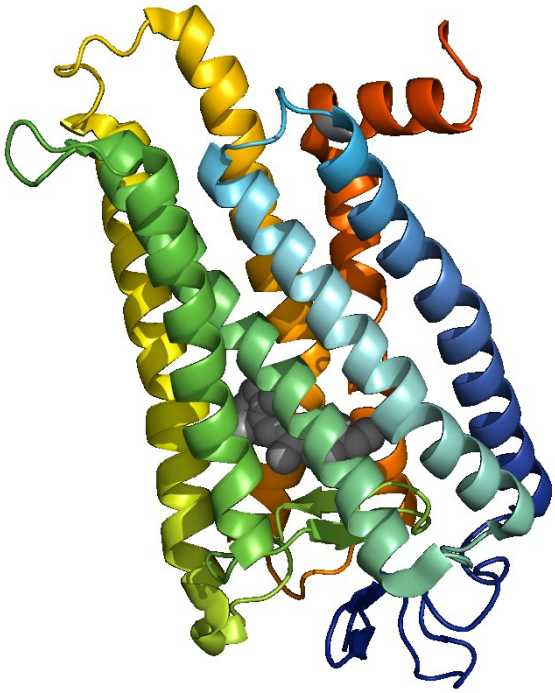

Figure 2: Crystal structure of bovine rhodopsin (PDB: 1GZM). Helices are shown in rainbow order, with helix I in dark blue and helix VII in orange. The cytoplasmic surface is on top and the extracellular surface is on bottom in this representation.

The retinal chromophore (gray) is covalently bound to K296, which is located on helix VII (orange). Upon photoactivation, helix VI moves to reveal the G-protein binding location on the cytoplasmic surface. Figure 3 shows a side-by-side comparison of rhodopsin (*5*) and its activated state, metarhodopsin II (*4*).

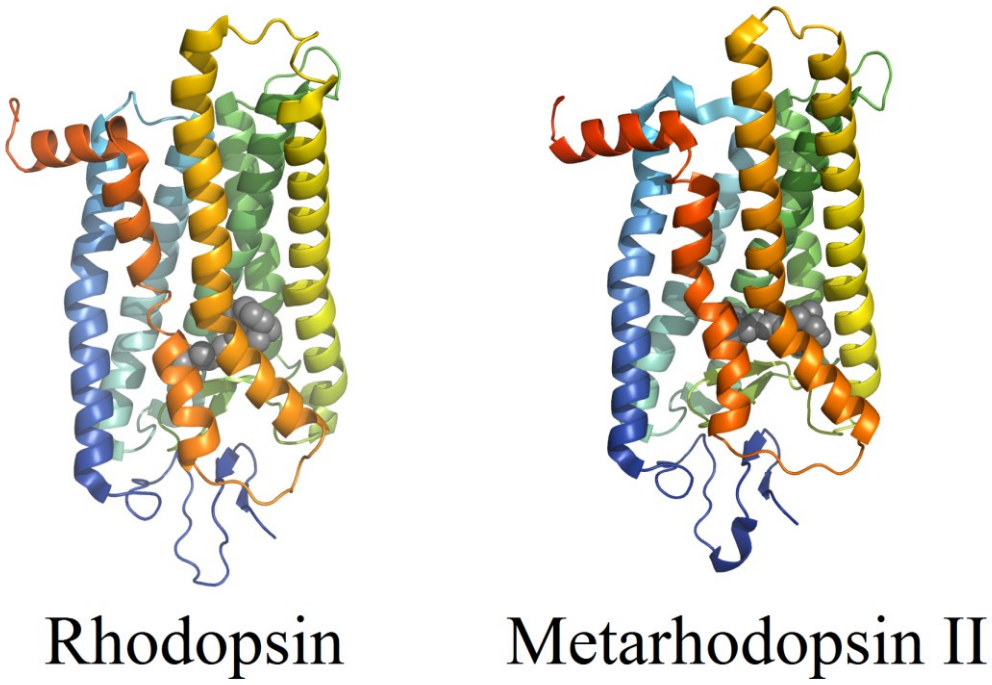

Figure 3: Crystal structures of rhodopsin (PDB: 1GZM) and metarhodopsin II (PDB: 3PXO)

1.3.2 Bovine Rhodopsin Photochemistry

Experiments using low-temperature trapping of photolysis intermediates demonstrated that rhodopsin activation proceeds through several distinct

intermediates (*6*) (*7*) (*8*) (*9*) shown in Figure 4:

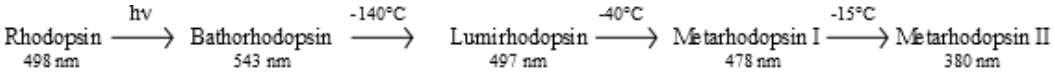

Figure 4: Low-temperature mechanism of bovine rhodopsin. Temperatures listed are the maximum temperature at which each intermediate is stabilized. The wavelength below each intermediate is the wavelength of maximum absorbance.

In the last few decades, fast optical methods have revealed intermediates that cannot be isolated by low-temperature trapping (*10*) (*11*) (*12*) (*13*). Room temperature time-resolved absorption experiments have shown that the activation mechanism cannot be explained by a simple sequential reaction scheme. The current model for rhodopsin activation is shown below in Figure 5:

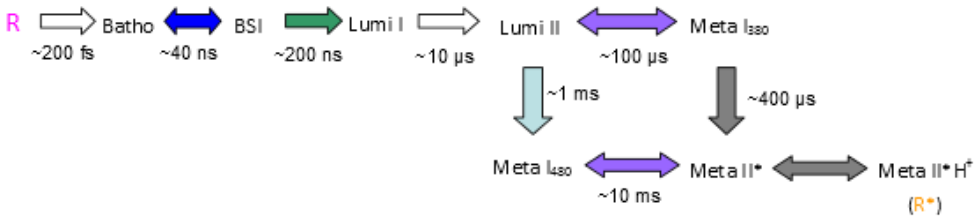

Figure 5: Room-temperature mechanism of bovine rhodopsin in membrane suspensions.

Rhodopsin has a primary absorbance band at 500 nm and a weaker transition at 340 nm due to its retinal chromophore. The first intermediate formed after isomerization is bathorhodopsin. It has an absorbance maximum red-shifted compared to rhodopsin, which is thought to arise from the torsional strain that comes from forcing

all-*trans* retinal into a binding pocket optimized for 11-*cis* retinal. This torsional strain is relieved somewhat as bathorhodopsin equilibrates with the next intermediate on the activation pathway, BSI (blue-shifted intermediate). After a few hundred nanoseconds, lumirhodopsin I is produced. Lumirhodopsin I is relatively stable, not decaying until several microseconds has passed. It has an absorbance maximum around 490 nm, which is thought to be due to changes in the hydrogen bond network. Lumirhodopsin I then forms an equilibrium with lumirhodopsin II. Since lumirhodopsin II was only recently discovered (*11*), it is not clear what structural differences exist between the two lumirhodopsins. They have very similar absorption spectra, but may show some differences in their circular dichroism spectra (*14*). Lumirhodopsin II formation is notable as the last detergent-independent process known in rhodopsin at room temperature (*15*). Later processes in the bleaching sequence are strongly perturbed in the presence of detergent; detergent-solubilized samples of rhodopsin show no sign of metarhodopsin I_{480}, instead being entirely shifted towards the metarhodopsin I_{380} pathway. When prepared in the native disk membrane, lumirhodopsin II has two possible pathways. It establishes an equilibrium with metarhodopsin I_{380} in about 100 microseconds, which irreversibly becomes metarhodopsin II in a few hundred more microseconds. Alternatively, lumirhodopsin II can in milliseconds irreversibly form metarhodopsin I_{480}, which then is in equilibrium with metarhodopsin II. Metarhodopsin I_{380} and metarhodopsin I_{480} differ in the protonation state of the Schiff base; metarhodopsin I_{480} remains protonated while metarhodopsin I_{380} is deprotonated. The relative amounts of metarhodopsin I_{380}

and metarhodopsin I_{480} formed are determined by the conditions under which rhodopsin is studied. High pH and low temperature push rhodopsin towards metarhodopsin I_{480}, while low pH and high temperature favor metarhodopsin I_{380} (*12*) (*16*). Once metarhodopsin II is formed, it also exists in equilibrium between deprotonated (metarhodopsin II_a) and protonated (metarhodopsin II_b) states (*17*); the protonated form is the active signaling state.

1.4 Human Rhodopsin

Bovine rhodopsin has been extensively characterized, since it is readily obtained from commercial sources in large quantities. Human rhodopsin, while more directly relevant to human vision, is more difficult to acquire in large amounts, so its mechanism has not been explored as thoroughly. Human and bovine rhodopsin share 93% sequence identity (*2*), so the photochemistry is thought to be largely similar. However, near the retinal binding site, human rhodopsin has A298 while bovine has S298. In the bovine crystal structure, S298 forms a hydrogen bond to the protein backbone, which the human A298 cannot do. This could potentially impact the flexibility of the binding pocket, which could lead to different rates in the human rhodopsin bleaching mechanism. In order to understand the details of human rhodopsin activation and how comparable its mechanism is to bovine rhodopsin, human rhodopsin needs to be studied directly.

1.4.1 Previous work

The nanosecond kinetics of human rhodopsin were studied in 1991 using time-resolved optical absorbance (TROA) spectroscopy and compared to bovine rhodopsin (*18*). The kinetic data for both human and bovine rhodopsin could be fit with the same kinetic scheme shown in Figure 6, but with somewhat different time constants. In this time regime, bovine rhodopsin forms an equilibrated mixture of bathorhodopsin and BSI with a time constant of 36 ns, followed by decay to lumirhodopsin in 215 ns. Human rhodopsin follows the same pathway, but with time constants 65 ns and 292 ns, considerably slower than in bovine rhodopsin.

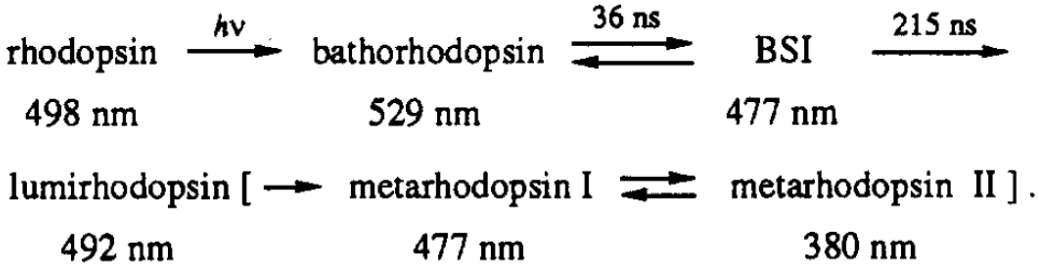

Figure 6: Kinetic model of bovine rhodopsin used to interpret the nanosecond intermediates (17)

The same study also examined the microsecond and millisecond kinetics of human rhodopsin. The human and bovine TROA difference spectra were largely similar, validating the use of bovine rhodopsin as a good model for human rhodopsin. However, there were some subtle differences between the two proteins. The metarhodopsin I - metarhodopsin II equilibrium constant appeared to be larger in human rhodopsin than in bovine rhodopsin. At the time these studies were

conducted, only one metarhodopsin I species was identified and the branching mechanism was unknown. These kinetic differences were tentatively attributed to human rhodopsin having somewhat more compact side chains than bovine rhodopsin in the transmembrane regions.

Since that time, there have been considerable advances in characterizing bovine rhodopsin. The kinetic scheme has been significantly refined with the identification of lumirhodopsin II and metarhodopsin I_{380}. There are now several crystal structures of bovine rhodopsin, so the impact of the sequence differences between human and bovine rhodopsin can be evaluated in light of a reference structure. With this additional structural and mechanistic information gained from the past two decades of bovine rhodopsin research, it is time to revisit the mechanism of human rhodopsin activation. The microsecond and millisecond kinetics of human rhodopsin have not been interpreted in terms of all of the currently known bovine intermediates. Lumirhodopsin II is a promising candidate for study in human rhodopsin, since it can be studied over a relatively narrow timescale. It is also the last detergent-independent intermediate, at least in bovine rhodopsin, so any differences between human and bovine rhodopsin can be attributed to the protein alone. After lumirhodopsin II, the rest of the mechanism can be explored up to metarhodopsin II. This will require a study at several time points, which will produce broad information on how well the bovine mechanism can be applied to human rhodopsin.

Chapter 2: Experiments

2.1 Materials and Methods

Crude human rod outer segments (ROS) had been previously obtained from donated eyes used for corneal transplants (*19*). These rod outer segments were further purified by hypotonic washing to remove extrinsic membrane proteins. The crude ROS were twice resuspended in a 1 mM, pH 7 EDTA solution and pelleted by centrifugation at 17,000 rpm for 45 minutes using a Sorvall SS-34 rotor. The ROS were then washed with Tris-buffered saline (TBS: 10 mM Tris, 60mM KCl, 30 mM NaCl, 2 mM $MgC1_2$, 0.1 mM EDTA, pH 7) and resuspended in TBS at a final concentration of approximately 1 mg/mL. The purified human rhodopsin was then stored at -70°C for use in time-resolved absorption experiments.

Bovine rhodopsin was prepared from dark-adapted bovine retinas as described previously (*20*). Rod outer segments were detached from the retinas by shaking for approximately one minute. The ROS were then separated by a sucrose density gradient. A solution of 43% sucrose in Tris-buffered saline (TBS) with 0.01 trypsin inhibitor unit of aprotinin and 1 mM fresh dithiothreitol was added to the ROS followed by centrifugation (5,000 rpm, 5 minutes). The supernatant was collected, mixed with TBS, and centrifuged for 15 minutes at 15,000 rpm. The pellets were resuspended in a solution of 33% sucrose in TBS, and then the sucrose concentration was adjusted to 32.5% (as measured by refractive index) by adding 43% sucrose in TBS. The suspension was then centrifuged for 4 hours at 8,000 rpm. After the centrifugation, rhodopsin harvested carpets were collected from the sucrose-TBS

interface with a course-gauged syringe and stored at -70°C. The harvested carpets were hypotonically washed to remove the extrinsic membrane proteins. The crude ROS were twice resuspended in a 1 mM, pH 7 EDTA solution and pelleted by centrifugation at 17,000 rpm for 45 minutes. The ROS were then washed with TBS and resuspended in TBS at a final concentration of approximately 1.5 mg/mL and stored at -70°C.

2.2 Experimental Apparatus

TROA difference spectra were obtained using a pump-probe absorbance apparatus described previously, except that the optical multichannel array detector was replaced with an intensified charge-coupled device (iCCD) (*21*). A block diagram of the time-resolved optical absorption (TROA) apparatus is shown in Figure 7 below. The protein sample was excited by a 7 ns pulse of vertically polarized 477 nm light from a dye laser pumped by the third harmonic of a Nd:YAG laser system (355 nm). The excitation beam had fluence of approximately 50 $\mu J/mm^2$, with a sample pathlength of 0.5 mm. White probe light from approximately 200 nm to 700 nm was generated by a discharge from a xenon flash lamp. The probe light was collimated and passed through a polarizer, which in these experiments was fixed at 54.7° from vertical to eliminate potential artifacts from rotational diffusion, which in membrane suspensions occurs on the order of microseconds (*22*). The probe light was then focused onto the 2 mm pathlength sample cell, and then recollimated and refocused into a spectrograph and captured by an intensified charge-coupled device, where the spectrum was recorded. Each laser measurement was preceded by probing

the sample with white light alone in order to obtain a reference transmission spectrum. The time delay between the pump and probe beams was controlled by an electronic delay generator. Between each flash, a small (approximately 1 μL) amount of rhodopsin was pumped by a syringe pump into the sample cell. This removes most of the previously bleached protein and also ensures that the sample contains a consistent amount of unbleached sample for probing.

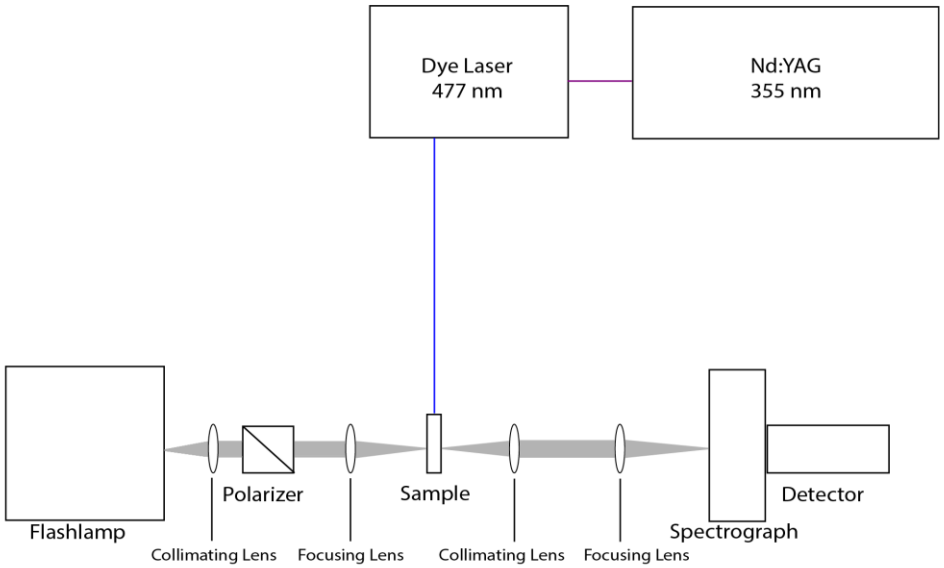

Figure 7: Block diagram of the TROA apparatus

2.3 Data Analysis

The TROA difference spectra acquired throughout this project were analyzed by singular value decomposition (SVD) followed by global exponential fitting. SVD is a mathematical procedure wherein a matrix of data A(λ,t) is decomposed into

orthogonal components that satisfy $A(\lambda, t) = \boldsymbol{USV}^T$, where **U** and **V** are matrices of the spectral and temporal components, respectively, and **S** is a diagonal matrix of the singular values that represent the relative importance of each component. The power of SVD lies in its ability to pick out more significant patterns in the data and discard components that contribute only noise. The SVD-filtered data was then fit to a sum of exponential functions as

$$A(\lambda, t) = b_0(\lambda) + b_1(\lambda)e^{-\frac{t}{\tau_1}} + b_2(\lambda)e^{-\frac{t}{\tau_2}} + \cdots$$

where the b_i are the spectra coefficients and the τ_i are the time constants associated with their corresponding *b*-spectra.

In the general case, the *b*-spectra are a convenient model-independent mathematical description without a physical meaning of their own. However, when combined with a proposed kinetic scheme, the *b*-spectra and time constants can be related to intermediate spectra and microscopic rate constants. In the case of a sequential first-order mechanism with no back reactions, such as $A \xrightarrow{k_1} B \xrightarrow{k_2} C \xrightarrow{k_3} D$, the rate of change of the intermediates can be written in matrix form as

$$\frac{d}{dt}\begin{bmatrix} A \\ B \\ C \\ D \end{bmatrix} = \begin{bmatrix} -k_1 & 0 & 0 & 0 \\ k_1 & -k_2 & 0 & 0 \\ 0 & k_2 & -k_3 & 0 \\ 0 & 0 & k_3 & 0 \end{bmatrix}\begin{bmatrix} A \\ B \\ C \\ D \end{bmatrix}$$

or more compactly, $\frac{d}{dt}E = \boldsymbol{K}E$, where **K** is called the kinetic matrix and E is a column vector of the concentrations of the intermediate species. The solution to this set of first-order differential equations is $E(t) = \boldsymbol{a}T$, where $T_i = e^{-r_i t}$, **a** is the matrix of eigenvectors of **K**, and the r_i are the eigenvalues of **K**. The r_i, in addition to their

role as eigenvalues, are also the apparent rates that would be obtained from an exponential fit – the very same rates associated with the *b*-spectra. The *b*-spectra are related to the kinetic matrix through $b = E\boldsymbol{a}$, so with the *b*-spectra from the exponential fitting, and the eigenvector matrix from the rate constants, the intermediate spectra *E* can be calculated directly.

2.4 Sample Integrity

2.4.1 Absorption Spectra

The human rhodopsin samples had been frozen as harvested carpets for some time, so the first task was to verify that that the protein was still intact. The standard method of checking rhodopsin quality and purity is the absorbance spectrum before and after photobleaching. The difference in absorbance at 500 nm between unbleached and bleached rhodopsin is due to rhodopsin photoactivation, giving a quantitative measure of how much rhodopsin is present and capable of activation. A 100 µL sample of human rhodopsin with optical density of approximately 0.4 was diluted by a factor of ten in 3% Ammonyx detergent to reduce the turbidity due to the disk membrane present. After recording the ultraviolet-visible absorbance spectrum, the rhodopsin was then bleached for approximately 30 seconds with a bright fluorescent lamp. The spectrum of the bleached rhodopsin was then recorded. Figure 8 shows the static absorbance spectrum of human rhodopsin before and after bleaching as well as the difference. The static absorbance spectrum shows considerable light scattering, which is not surprising since the human rhodopsin

sample had a large amount of disk membrane remaining. The feature around 360 nm is an artifact due to the spectrophotometer switching light sources. The difference spectrum has a maximum value of 0.029 near 500 nm, corresponding to an original rhodopsin concentration of 2.9 mg/mL in the undiluted aliquot. The ratio of absorbance at 280 nm and 500 nm (A_{280}/A_{500}) is used to characterize the purity of a rhodopsin sample, since the presence of other proteins would contribute to the absorbance at 280 nm but not 500 nm. The A_{280}/A_{500} ratio for this preparation is approximately 6, which would typically indicate the presence of other proteins. However, the significant light scattering present in the human rhodopsin samples is expected to exaggerate the extinction at shorter wavelengths, so the rhodopsin is likely to be more pure than this ratio would otherwise indicate.

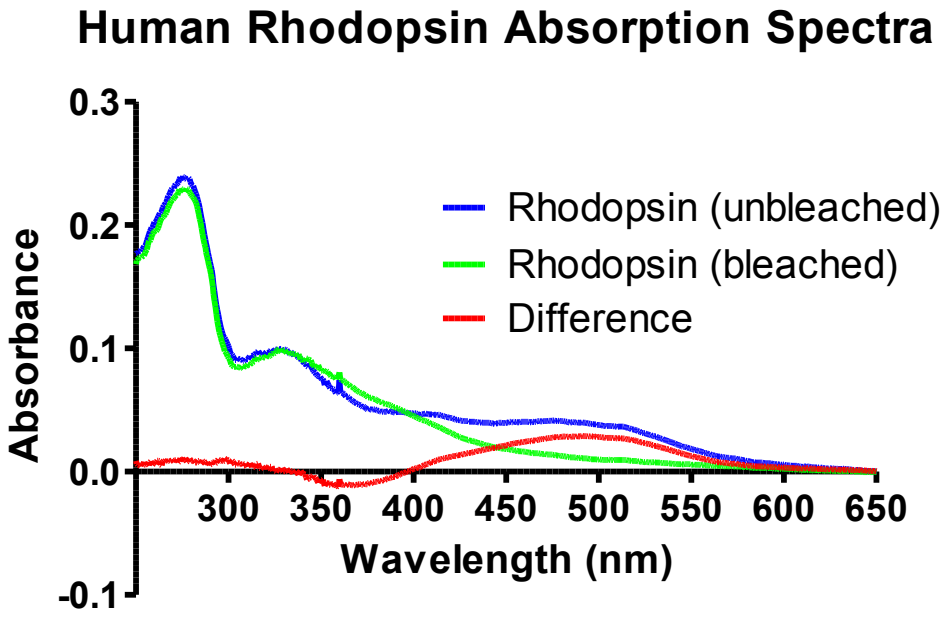

Figure 8: Absorbance spectrum of human rhodopsin before and after photobleaching.

2.4.2 Kinetics

To check for membrane degradation, which would impact the kinetics but not the static spectrum, we repeated the previous time-resolved difference absorption experiment with the human rhodopsin. On the day of the experiment, 1 mL of human rhodopsin at approximately 1 mg/mL was allowed to thaw to room temperature. The sample was centrifuged at 12,000 rpm for 20 minutes and the supernatant was removed. The remaining pellet was resuspended in 1 mL of buffer (10 mM Tris, 2 mM $MgCl_2$, 0.1 mM EDTA, pH 7.0). The solution was then lightly sonicated under argon (30 seconds sonication, followed by 30 seconds off) three times in order to reduce the light scattering due to the disk membranes. TROA difference spectra were

recorded at delay times from 1 µs to 101 ms (1 and 10 µs, and 2, 6, 10, 20, and 101 ms). The measured TROA difference spectra were unchanged from those reported in 1991 (*18*), so the human rhodopsin was presumed intact and suitable for further study (Figure 9).

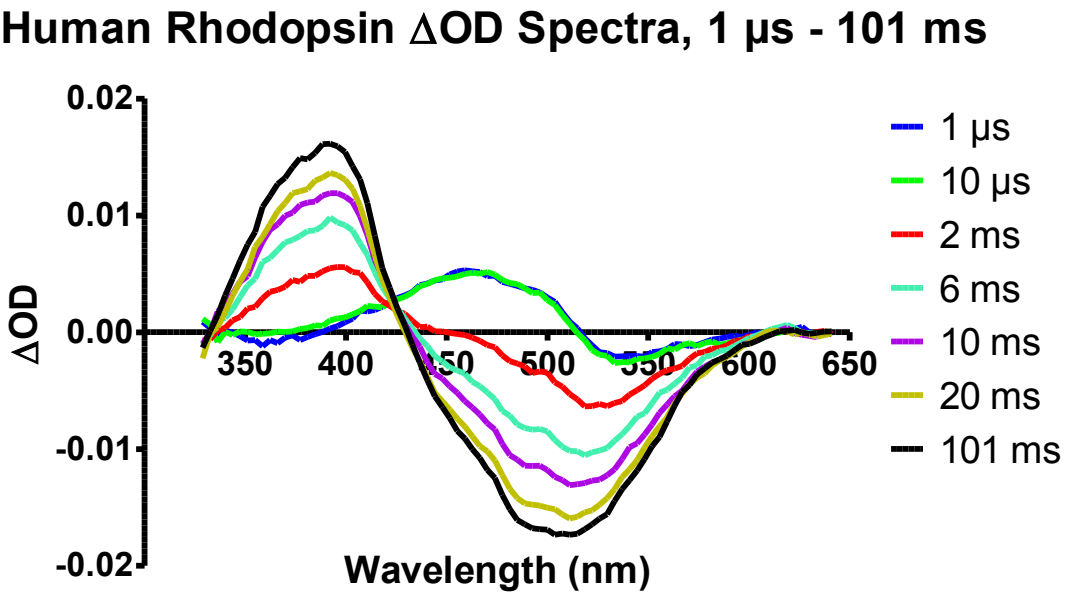

Figure 9: Human rhodopsin TROA difference spectra from 1 µs to 101 ms.

2.5 Lumirhodopsin

In bovine rhodopsin, an equilibrated mixture of lumirhodopsin I and II forms from lumirhodopsin I with a time constant of 12 µs at pH 7 and 20°C (*15*). Lumirhodopsin II had not yet been discovered at the time human rhodopsin was previously studied, so no prior information exists on whether the formation of this intermediate occurs in the same time regime as in bovine rhodopsin, or if it even

exists in the human rhodopsin activation mechanism. Previous work on the nanosecond intermediates of human rhodopsin had shown that the human protein follows the same general scheme as bovine rhodopsin, but with slower time constants (*18*). Assuming that this trend holds for the microsecond processes as well, we decided to study human lumirhodopsin II using the same strategy as was used for bovine rhodopsin.

2.5.1 Methods

Human rhodopsin was hypotonically washed in TBS buffer at pH 7 as described above. On the day of each experiment, approximately 1 mg of rhodopsin was removed from -70°C storage and allowed to thaw to room temperature. The rhodopsin was then spun down via centrifugation at 12,000 RPM for 20 minutes. The supernatant was removed and the rhodopsin was resuspended in 1 mL of TBS buffer at pH 7. The rhodopsin was then gently sonicated under argon (30 seconds of sonication followed by 30 seconds of rest for a total of three sonication cycles) in order to reduce the turbidity of the solution and then allowed to settle for 30 minutes. Subsequently, the rhodopsin solution was degassed under house vacuum at room temperature and loaded into the syringe pump of the microscale absorption apparatus. TROA difference spectra were recorded at logarithmically spaced delay times from 1 μs to 128 μs (1, 2, 4, 8, 16, 32, 64, and 128 μs) measured from the end of the laser pulse to the opening of the iCCD gate. A gate width of 1.5 μs was used due to the high turbidity of the human rhodopsin membrane samples. The temperature was controlled at 20°C by use of a water bath circulating through a copper block around

the sample chamber. The probe polarizer was set to magic angle (54.7° relative to the vertically polarized laser) to eliminate artifacts arising from rotational diffusion.

2.5.2 Results

The TROA difference spectra are presented in Figure 10. The spectrum at each delay time is the average of 256 individual measurements. The delay spectra show the decay of rhodopsin into lumirhodopsin, followed by a minor increase in the ultraviolet absorbance accompanied by a loss of visible absorbance. Singular value decomposition (SVD) followed by exponential fitting produced the *b*-spectra in Figure 11, with time constants 1.39 μs and 33.2 μs. For comparison, the corresponding *b*-spectra for bovine rhodopsin have time constants 11 μs and 90 μs (*15*). The human b_1 spectrum is of dubious quality and may reflect fast light scattering changes. The b_2 spectrum is similar to the bovine b_1 spectrum, which is primarily assigned to the lumirhodopsin I – lumirhodopsin II difference spectrum. This suggests that lumirhodopsin II does exist in human rhodopsin, but forms considerably more slowly than in bovine rhodopsin. A more detailed analysis is complicated by the subsequent formation of a 380 nm product, which would also need to be included if it occurs on a similar timescale. There are significant artifacts present in the ultraviolet region, particularly at 4 μs and 16 μs, due to a laser-induced thermal shockwave. These artifacts are not present in water, so a simple baseline subtraction was ineffective at compensating for these artifacts. The poor ultraviolet data at those time delays hinder a straightforward determination from this experiment alone of when metarhodopsin I_{380} may be forming. This shockwave is sensitive to the

specific time delay used, so future experiments use modified delay times to avoid most of this distortion. In order to more concretely confirm the existence of lumirhodopsin II and further explore the differences between human and bovine rhodopsin, it was decided to extend the human rhodopsin studies to encompass the rest of the mechanism up to metarhodopsin II.

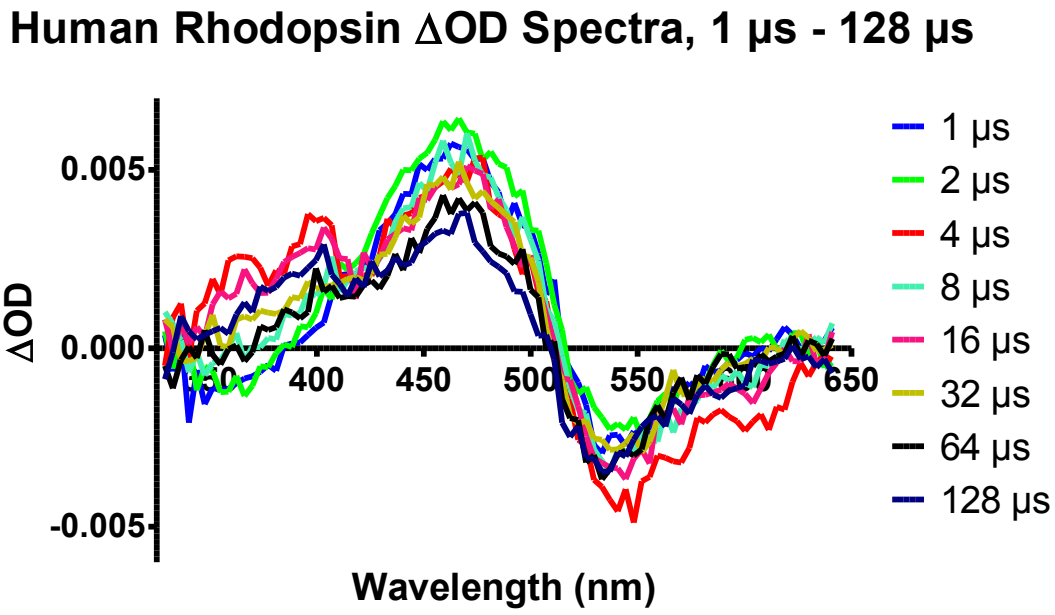

Figure 10: Human TROA difference spectra from 1 µs to 128 µs at pH 7 and 20°C.

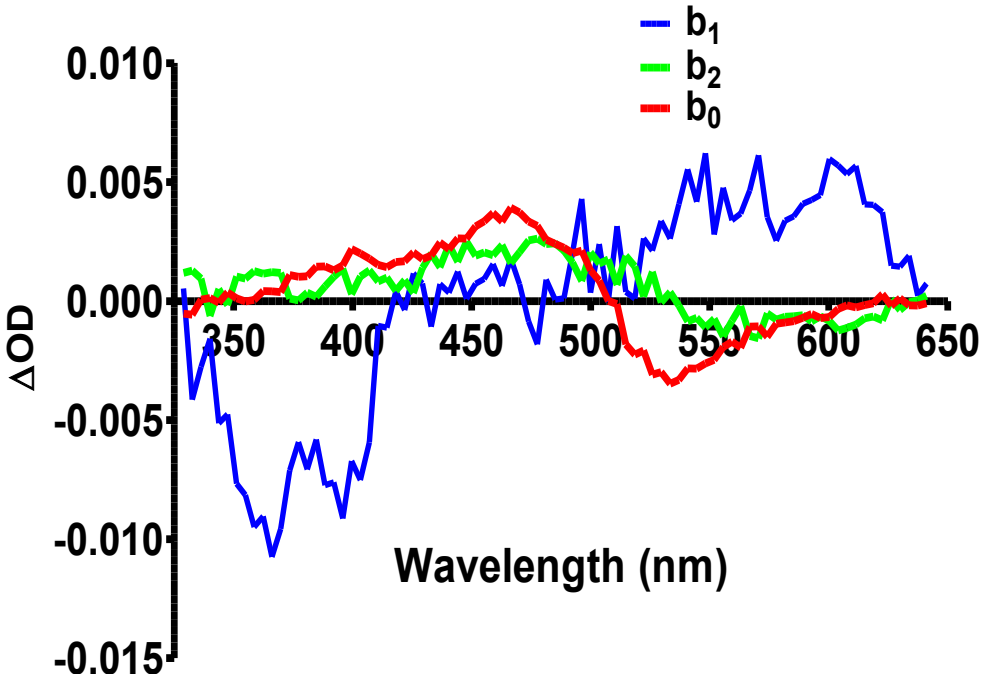

Figure 11: Human rhodopsin b-spectra from a two-exponential fit. The lifetimes obtained were 1.39 μs and 33.2 μs for b_1 and b_2, respectively.

2.6 Rhodopsin Activation Mechanism: Preliminary Experiment

The mechanism for bovine rhodopsin activation can proceed through either metarhodopsin I_{380} or metarhodopsin I_{480} (as shown in Figure 5). Metarhodopsin I_{380} is in equilibrium with lumirhodopsin II and forms quickly, within hundreds of microseconds. Upon its formation, metarhodopsin I_{380} irreversibly decays to metarhodopsin II in a few hundred microseconds. Lumirhodopsin II can also decay to metarhodopsin I_{480} irreversibly. This is a slower process, with a time constant of approximately one millisecond. Metarhodopsin I_{480} then equilibrates with

metarhodopsin II. The two equilibrium constants (lumirhodopsin II – metarhodopsin I_{380} and metarhodopsin I_{480} – metarhodopsin II) together determine whether the rhodopsin photochemistry proceeds directly to 380 nm product, passes through a 480 nm intermediate on the way to activation, or ends up with primarily a 480 nm product. These equilibria are governed by the reaction conditions, notably temperature, pH, and the presence of a detergent. When rhodopsin is solubilized in detergent, only a 380 nm product is observed: essentially no metarhodopsin I_{480} forms. When rhodopsin is in its native membrane, the relative amounts of metarhodopsin I_{380} and metarhodopsin I_{480} are governed by a pH- and temperature-sensitive equilibrium. At higher temperatures, metarhodopsin I_{380} is formed preferentially to metarhodopsin I_{480}, which is observed the TROA difference spectra as the formation of a peak at 480 nm rather than 380 nm. In bovine rhodopsin, 30°C is sufficient to shift the equilibrium enough so that metarhodopsin I_{380} and metarhodopsin II dominate and very little metarhodopsin I_{480} is observed. Lower pH has a similar effect. In contrast, high pH and low temperature favor metarhodopsin I_{480}. At 15°C and pH 8.7, for instance, bovine rhodopsin produces metarhodopsin I_{480} nearly exclusively; not even metarhodopsin II is formed in appreciable amounts. Human rhodopsin is expected to follow similar trends, although this has not been directly verified until this study. To elucidate the mechanism of human rhodopsin, we investigated the activation mechanism at 15°C and 30°C at pH 8.7. These conditions are not physiological, but allow all of the intermediates to be observed.

2.6.1 Methods

Hypotonically washed human rhodopsin was prepared as described above. Similar to the experiments described previously, on the day of an experiment, approximately 1 mg of rhodopsin was thawed to room temperature and centrifugated for 20 minutes at 12,000 rpm. The supernatant was removed and the rhodopsin pellet resuspended in BTP buffer (10 mM Bis-tris propane, 100 mM NaCl) at pH 8.7 and lightly sonicated as before (30 seconds of sonication followed by 30 seconds of rest, repeated a total of three times). Temperature was held constant at 15°C or 30°C by means of a copper insert connected to a water bath. Human rhodopsin TROA difference spectra were taken on the microscale TROA apparatus described previously. Preliminary delay times were chosen to match the times from comparable bovine rhodopsin experiments, ranging from 10 μs to 240 ms (at 15°C) or 20 ms (at 30°C). At 15°C, absorption spectra were acquired at 10 μs, 100 μs, 200 μs, 500 μs, 1 ms, 2 ms, 5 ms, 10 ms, 20 ms, 50 ms, 120 ms, and 240 ms. The delay times at 30°C were 10 μs, 40 μs, 80 μs, 160 μs, 320 μs, 640 μs, 1.28 ms, 2.56 ms, 5.12 ms, and 20.48 ms.

2.6.2 Results

The TROA difference spectra of human rhodopsin on the microsecond to millisecond time scale are presented in Figures 12 (15°C) and 13 (30°C). The delay times used were chosen based on previous work of bovine rhodopsin. The 15°C spectra shown are the averages of 48 individual measurements. The 30°C spectra,

due to the larger signal from the forward-shifted equilibria, are the averages of 16 measurements.

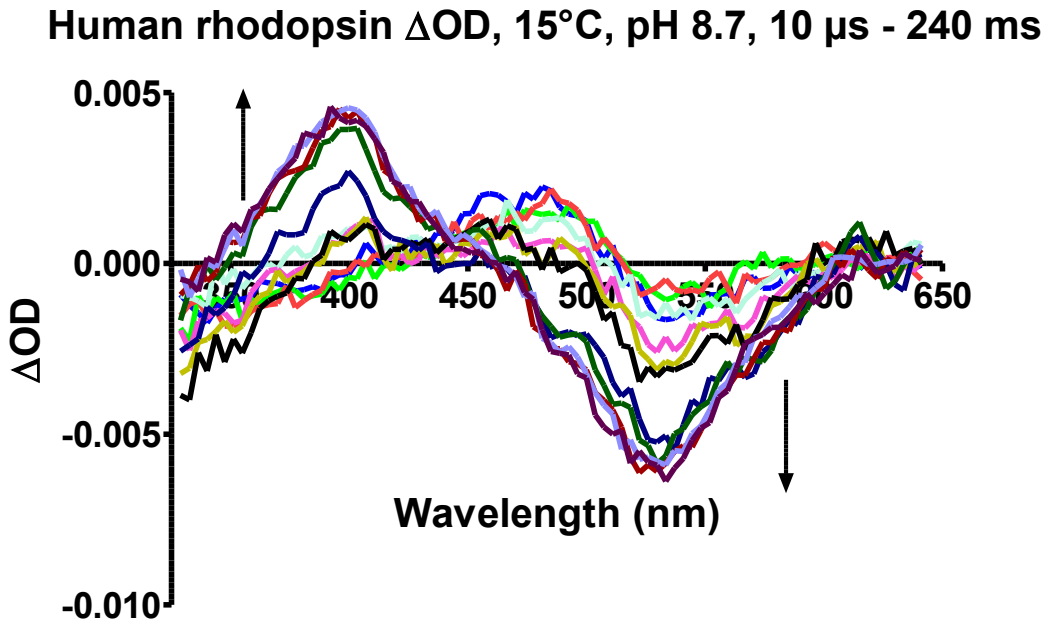

Figure 12: Human rhodopsin TROA difference spectra from 10 µs to 240 ms at 15°C and pH 8.7.

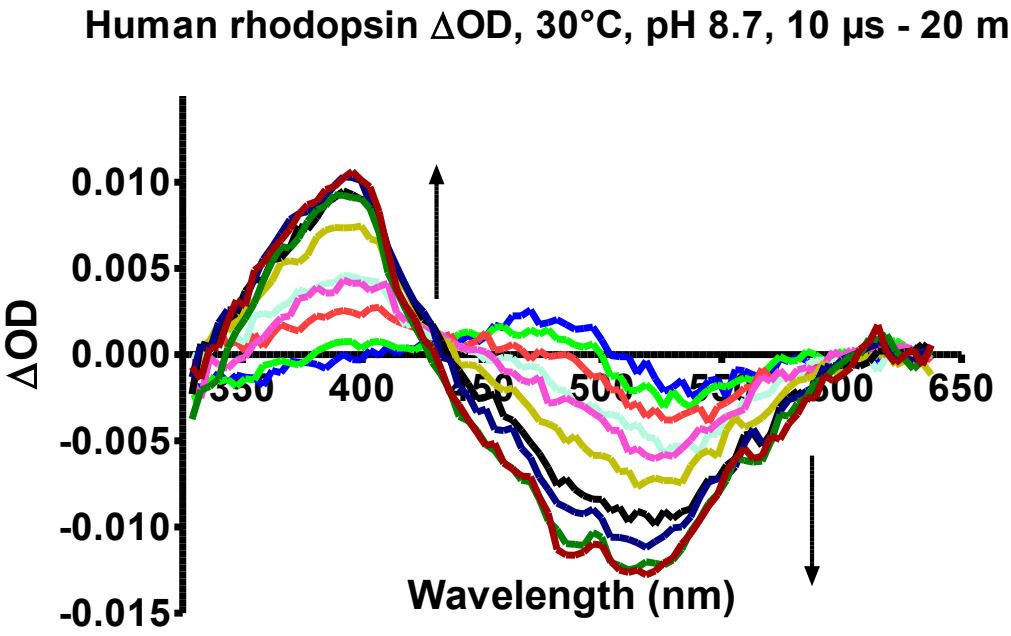

Figure 13: Human rhodopsin TROA difference spectra from 10 µs to 20 ms at 30°C and pH 8.7.

At 30°C, the equilibria are very forward-shifted, even at high pH; almost no 480 nm product was formed. At 15°C, there is clear evidence of both a 480 nm intermediate and a 380 nm product. This is in stark contrast to bovine rhodopsin, which at 15°C forms predominately a 480 nm product. Human rhodopsin at pH 7 displays more 380 nm product than bovine rhodopsin, so this is not an unexpected result. Since human rhodopsin at pH 8.7 and 15°C appears to display all of the intermediates found in the bovine rhodopsin mechanism, the rest of this work will focus on this set of conditions. The preliminary data suggest some refinements for the delay times; since there is essentially no difference in the last three delay spectra,

the last time point can be omitted without loss of information. This time point can be replaced by a 5 μs time delay, which will be useful for fitting a poorly-resolved microsecond exponential process.

2.7 Rhodopsin Activation Mechanism: Refined Experiment

2.7.1 Methods

Human rhodopsin was prepared as previously described. Time-resolved difference absorption spectra were collected at delay times from 5 μs to 120 ms (5 μs, 10 μs, 30 μs, 50 μs, 100 μs, 500 μs, 1 ms, 2 ms, 5 ms, 20 ms, 50 ms, and 120 ms) at 15°C. Each time point is the average of 320 individual spectra. Additionally, a series of comparison experiments using bovine rhodopsin were conducted in order to verify that any differences between human and bovine rhodopsin are due to the different proteins. Bovine rhodopsin TROA difference spectra were recorded on the microscale TROA apparatus at 15°C using the same delay times as in the human rhodopsin experiments. Since the human rhodopsin had been previously bleached and regenerated, a portion of bovine rhodopsin was bleached and subsequently regenerated in the same way by incubating with 11-*cis* retinal followed by the addition of NADPH to reduce any excess retinal to retinol. To check for the effects of sonication on the rhodopsin kinetics, some of the bovine rhodopsin was lightly sonicated under argon using the same procedure as for the human rhodopsin.

2.7.2 Results

The human rhodopsin time-resolved absorption spectra are shown below in Figure 14. The first delay spectra show the formation of lumirhodopsin from rhodopsin. As the delay times increase, a product absorbing at 380 nm begins to form. The trough in the final delay spectrum is red-shifted relative to rhodopsin's 500 nm absorbance band, indicating the presence of a 480 nm product in addition to the 380 nm peak.

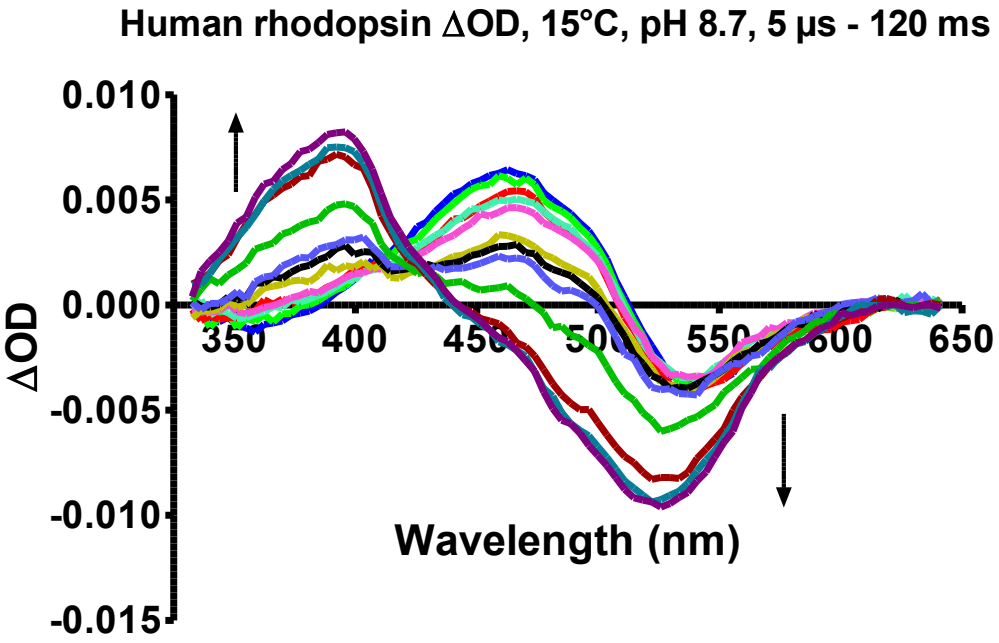

Figure 14: Human rhodopsin TROA difference spectra from 5 µs to 120 ms at 15°C and pH 8.7.

For comparison, bovine rhodopsin under the same conditions is presented in Figure 15. There is a clear difference in the later delay times. Bovine rhodopsin at low

temperature and high pH is known to primarily form a 480 nm product. This can be seen by a lack of any substantial peak at 380 nm, even after hundreds of milliseconds.

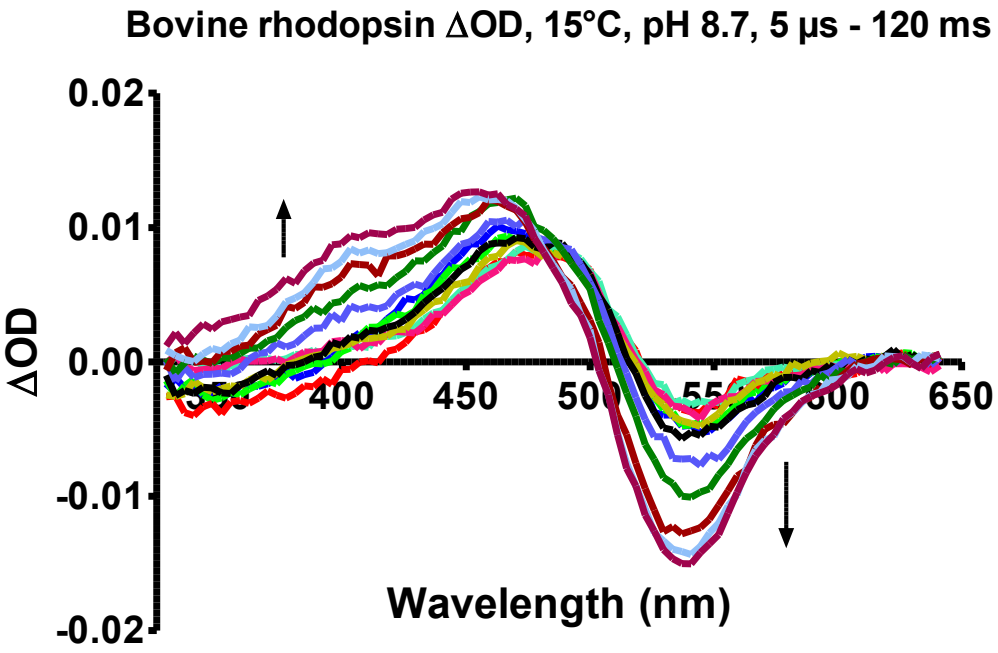

Figure 15: Bovine rhodopsin TROA difference spectra from 5 µs to 120 ms at 15°C and pH 8.7.

Figure 16 shows the TROA difference spectra of bovine rhodopsin under the same conditions, except that the rhodopsin had been previously bleached and regenerated. There is some increased 380 nm absorption at late delay times, suggesting that there is a minor perturbation in the kinetics due to rhodopsin regeneration. However, this effect is much smaller than the difference between human and bovine rhodopsin.

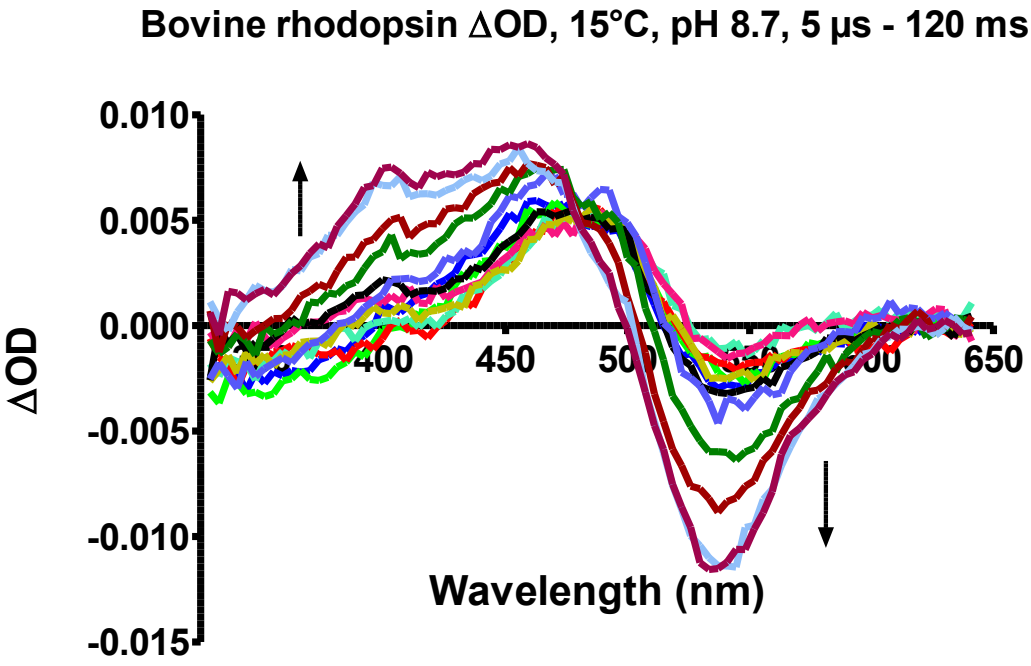

Figure 16: Regenerated bovine rhodopsin TROA difference spectra from 5 µs to 120 ms at 15°C and pH 8.7.

The rhodopsin absorption data were analyzed by SVD followed by global exponential fitting with three exponential components. The *b*-spectra for the human and bovine rhodopsin are shown in Figures 17 and 18. There are some major differences in the *b*-spectra, as would be expected considering the differences in the human and bovine time-resolved absorption spectra. The time constants for the human rhodopsin are considerably slower compared to the bovine rhodopsin, with 81.2 µs for b_1, 5.82 ms for b_2, and 31.3 ms for b_3 in human rhodopsin (12.5 µs, 2.10 ms, and 26.2 ms in bovine rhodopsin). This is most apparent in b_1, which is over 6 times slower in human rhodopsin. The human rhodopsin b_2 and b_3 are 2.8 and 1.2 times slower, respectively, than their bovine counterparts, but have very different spectral shapes.

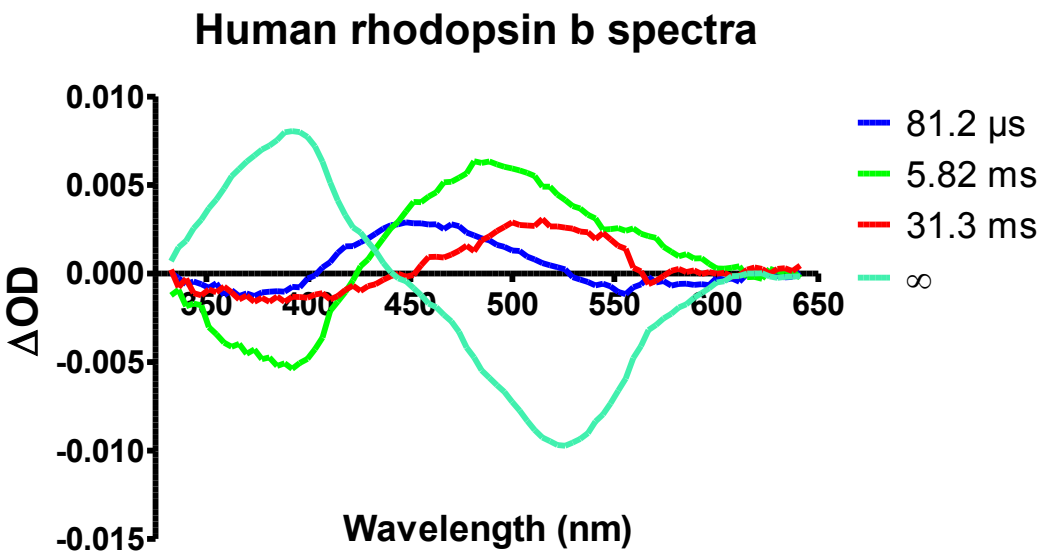

Figure 17: Three exponential fit of human rhodopsin TROA spectra at 15°C and pH 8.7.

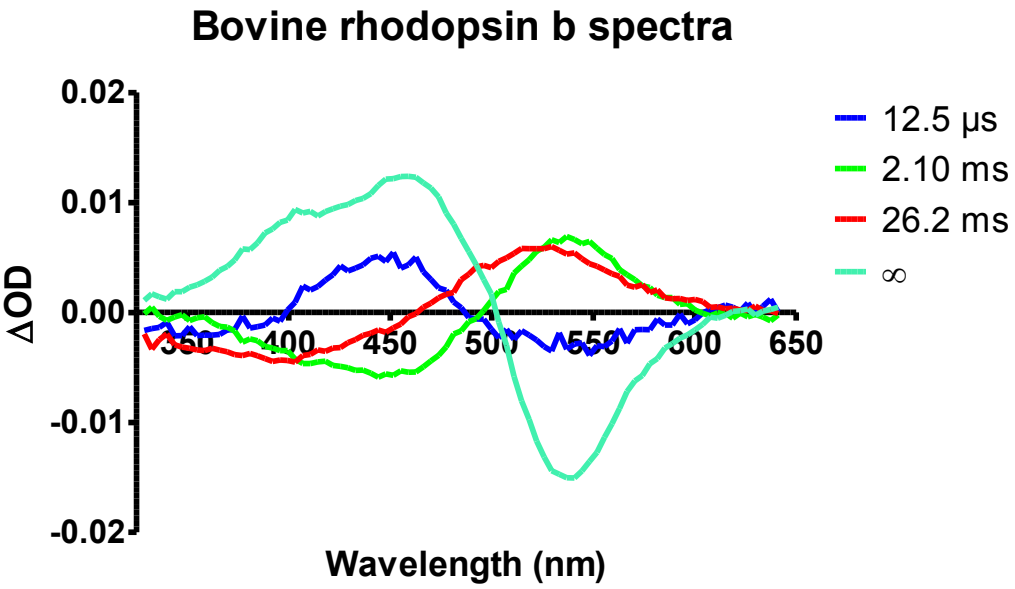

Figure 18: Three exponential fit of bovine rhodopsin TROA spectra at 15°C and pH 8.7.

2.7.3 Kinetic Analysis

In general, *b*-spectra cannot be directly assigned to a physical process. However, if the underlying physical changes are well-separated in time and the mechanism is sequential and irreversible, the *b*-spectra are approximately the spectral difference between successive processes. In the case of bovine rhodopsin, b_1 roughly corresponds to lumirhodopsin I becoming an equilibrated mixture of lumirhodopsin I and II. In b_2, the lumirhodopsins are converted into metarhodopsin I_{480}, while b_3 shows the final equilibration step between metarhodopsin I_{480} and the small amount of metarhodopsin II that forms. The final b_0 is the time-independent spectral term and reflects the final observed difference spectra after the time-dependent *b*-spectra have decayed. Human rhodopsin is complicated by the presence of a significant amount of metarhodopsin I_{380}, but the same general strategy applies. The human b_1 is spectrally largely similar to the bovine b_1, though there is a red shift in the crossing point from 500 nm to 530 nm. It is likely that the lumirhodopsin I – II equilibration process is convolved with the formation of metarhodopsin I_{380} in human rhodopsin. The time constant associated with the human rhodopsin b_1 is 81.2 μs, which is not very far removed from the approximately 100 μs for metarhodopsin I_{380} formation in bovine rhodopsin. With the large amount of metarhodopsin I_{380} formed in human rhodopsin, it quite probably contributes significantly to b_1, which complicates the analysis of the *b*-spectra in terms of simple difference spectra. The human b_2 and b_3 capture the formation of metarhodopsin I_{480} and metarhodopsin II much as in bovine, with the difference that much more metarhodopsin II is formed in human rhodopsin.

Since *b*-spectra are mathematical abstractions and not directly linked to a physical process, there is a limit to how much the data can be interpreted by examining the *b*-spectra alone. However, in the context of a kinetic scheme, it is possible to calculate the spectra of the intermediates from the *b*-spectra. Unlike *b*-spectra, these intermediate spectra are model-dependent, and thus must be interpreted with caution, because an incorrect kinetic mechanism will produce incorrect intermediate spectra.

The most straightforward approach to a kinetic model is a sequential scheme with no reverse reactions. The full rhodopsin mechanism clearly does not follow that sort of scheme. However, if groups of intermediates rather than pure intermediates are considered, it is possible to translate the much more complicated bovine rhodopsin mechanism into an approximately sequential scheme. Decomposing the human rhodopsin *b*-spectra into sequential intermediates produces the intermediate difference spectra shown in Figure 19. The absolute intermediate spectra are obtained by adding back the rhodopsin absorption spectrum (Figure 20). The corresponding concentration profiles are shown in Figure 21. The difference spectra so calculated represent the absorption of each intermediate (or collection of intermediate species) minus the original rhodopsin absorption. The initial difference spectrum can be attributed to lumirhodopsin I – rhodopsin, since the earliest delay times occur well after BSI decay (which takes place in hundreds of nanoseconds) but before lumirhodopsin II has a chance to form. The second intermediate difference spectrum could be a mixture of lumirhodopsin I and II with some metarhodopsin I_{380}.

Lumirhodopsin I and II primarily differ in extinction coefficient, so the absorption difference spectrum of a mixture of lumirhodopsin I and II minus rhodopsin as compared to pure lumirhodopsin I would primarily have a different amplitude. The intermediate difference spectrum observed here also has a positive band near 380 nm, which is very suggestive of the metarhodopsin I_{380} known to form on this timescale. The third and fourth intermediate difference spectra have very similar spectral shapes. There is a strong 380 nm band forming in both spectra, which, considering the timescale, is probably best attributed to metarhodopsin II. The trough in both spectra is red shifted past 500 nm, the primary rhodopsin absorption band, indicating the presence of a species with an absorption band near 480 or 490 nm. Since these intermediate mixtures form in milliseconds, metarhodopsin I_{480} is a much more likely candidate than either lumirhodopsin I or II. The third intermediate spectrum could represent the formation of an initially unequilibrated mixture of metarhodopsin I_{480} and metarhodopsin II. The fourth intermediate spectrum would then be the final equilibrated mixture of metarhodopsin I_{480} and metarhodopsin II.

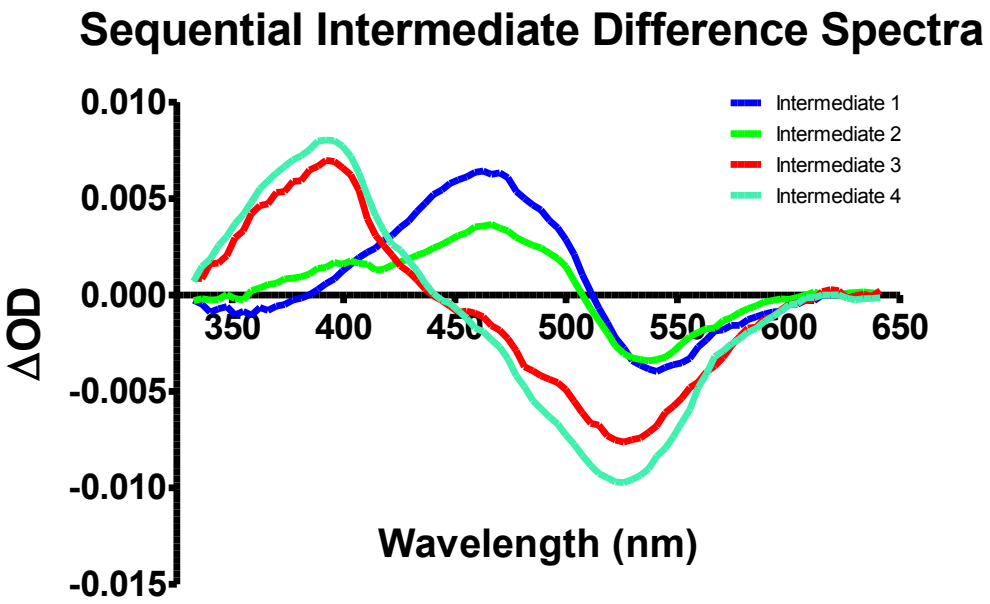

Figure 19: Sequential intermediate difference spectra for human rhodopsin at 15°C and pH 8.7.

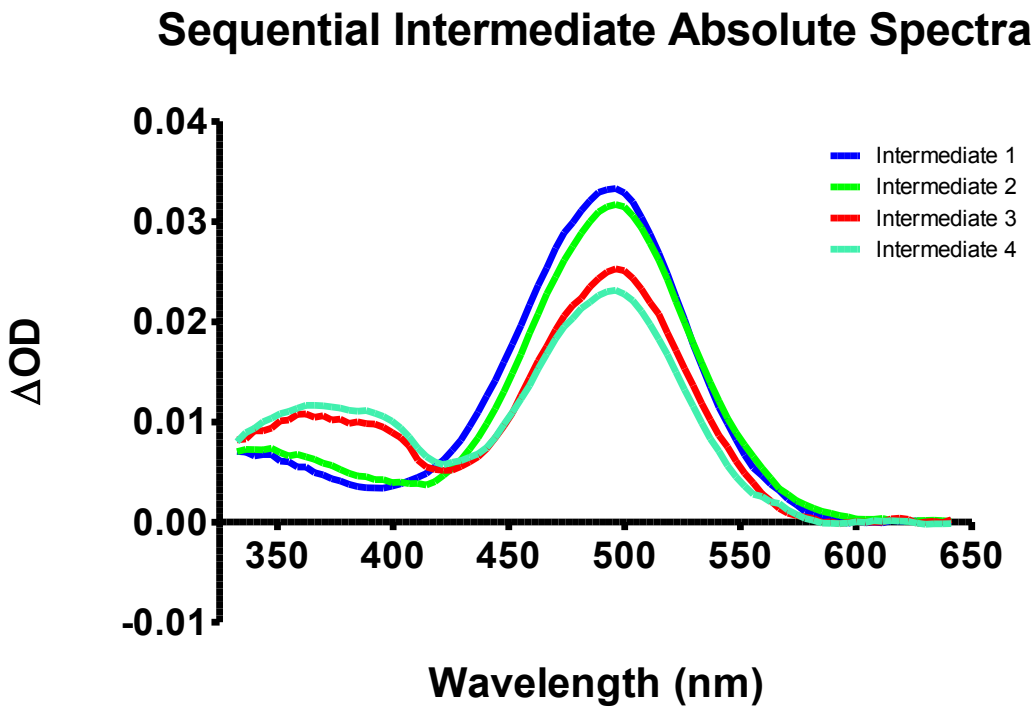

Figure 20: Sequential intermediate absolute absorption spectra for human rhodopsin at 15°C and pH 8.7.

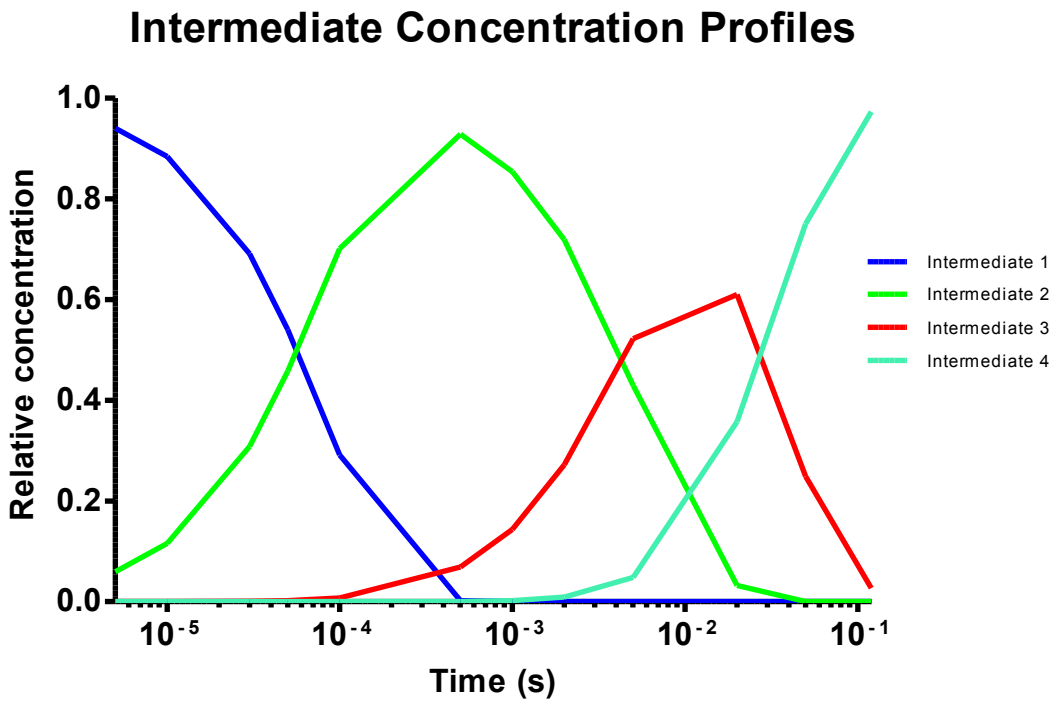

Figure 21: Concentration profile of the sequential intermediates calculated from the human rhodopsin b spectra.

In principle, it is possible to fit the absolute sequential intermediate spectra to combinations of the known rhodopsin intermediate spectra and thus determine how much of each intermediate is present at each time. This would allow a quantitative determination of the equilibrium constants and the microscopic rate constants for the rhodopsin activation mechanism. However, current efforts to model the sequential absolute spectra in terms of known bovine intermediates have proven unsuccessful. It is possible that the human intermediates have slightly shifted absorbance maxima compared to the bovine intermediates, which would cause difficulties in fitting the human time-resolved absorbance data satisfactorily.

2.7.4 Discussion

2.7.4.1 Kinetic differences

It is clear that human and bovine rhodopsin, while largely similar proteins, have some distinct differences in the details of their kinetic schemes. Previous work on the nanosecond intermediates of rhodopsin showed that human rhodopsin follows the same general pathway as bovine rhodopsin, but with slower rates. The microsecond and millisecond intermediates are more difficult to analyze in terms of a simple exponential fitting due to the branching scheme and equilibria, but there is a clear shift in the amount of 380 nm absorbing product formed in human rhodopsin. Human rhodopsin does appear to have all of the spectral intermediates seen in bovine rhodopsin. While the equilibrium is forward-shifted towards the 380 nm product compared to bovine rhodopsin, human rhodopsin does still demonstrate the temperature-dependent equilibrium, as can be seen in the 15°C and 30°C data. The analysis in terms of sequential intermediates can be interpreted in terms of the bovine mechanism, with significant production of metarhodopsin I_{380}. The lumirhodopsin I and II equilibrium is likely to be slower in human rhodopsin than in bovine rhodopsin, but because it occurs so close in time to metarhodopsin I_{380} production the two processes are difficult to separate. The final steps of metarhodopsin I_{480} and metarhodopsin II formation, followed by equilibration, are also subtly different in human rhodopsin. Deciphering the detailed differences in the microscopic rates requires a kinetic analysis that unfortunately is beyond the scope of this work.

However, it is clear from the apparent rates that human and bovine rhodopsin have similar intermediates with differing kinetics.

2.7.4.2 Structural differences

The kinetic measurements show that human and bovine rhodopsins have different rates for their photochemistry, but the question remains as to why the rates would differ at all. While the membrane interface could potentially be important for the last kinetic steps, in which helix VI shifts position, the early photochemistry, at least through lumirhodopsin, should depend primarily on the chromophore environment. It turns out that there are two amino acid differences near K296, which is where the retinal chromophore is attached. Human rhodopsin has S297 followed by A298, while bovine rhodopsin has T297 and S298. A threonine to serine mutation is unlikely to have much impact. A serine to alanine mutation, however, is a more significant change. With the advent of the rhodopsin crystal structure, it is possible to examine in detail the environment surrounding these residues. It turns out that in bovine rhodopsin, S298 is within hydrogen bonding distance of the backbone carbonyl of A295, as shown in Figure 22 below.

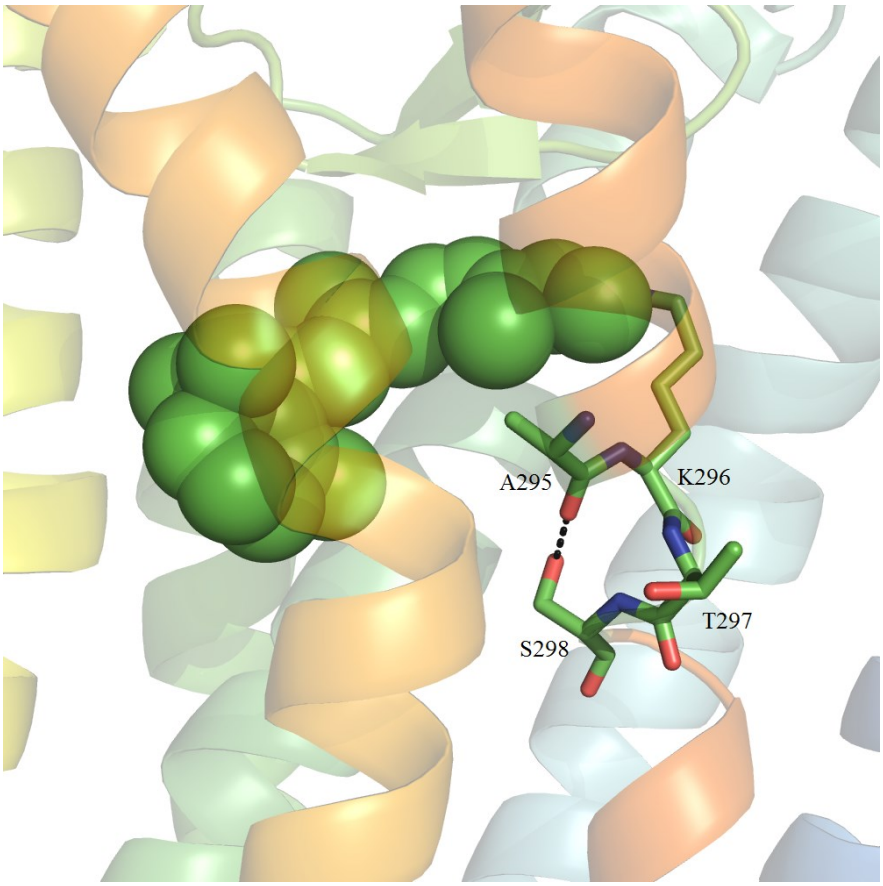

Figure 22: Chromophore binding environment in bovine rhodopsin.

It is difficult to make definitive claims about a hydrogen atom from a crystal structure, but it seems likely that S298 in bovine rhodopsin interacts with A295. There is no crystal structure of human rhodopsin for comparison, but since A298 does not have a hydroxyl side chain, the hydrogen bond to A295 is simply not possible. This may increase the flexibility in the chromophore binding pocket as compared to bovine rhodopsin. This change from S298 in bovine rhodopsin to A298 in human rhodopsin may serve to slow the early photochemistry in the latter. In bovine rhodopsin, the torsional strain on bathorhodopsin is the driving force pushing it

towards lumirhodopsin and the later intermediates – the binding pocket simply does not accommodate the all-*trans* chromophore very well. A more flexible chromophore region may help stabilize the human bathorhodopsin relative to its bovine counterpart and thus slow down its relaxation into BSI and lumirhodopsin. The later photochemistry probably cannot be attributed solely to differences in the binding pocket, since the metarhodopsin intermediates involve movements in the entire protein. The human sequence does have several smaller side chains in the transmembrane helices, as noticed previously (*18*). It is possible that these force the human rhodopsin into a more compact configuration, globally slowing down its late photochemical reactions.

Chapter 3: Final Thoughts

The work presented here demonstrates that the knowledge gained from studying bovine rhodopsin can be directly applied to human rhodopsin, confirming that bovine rhodopsin is a good model for studying the human protein. This study also highlights that there are indeed differences between the two proteins, so a full understanding of human rhodopsin does ultimately require studying it directly. Human rhodopsin appears to have the same set of intermediates as bovine rhodopsin, so the extensive studies on the bovine photochemistry and how it is controlled should still be relevant to the human protein.

3.1 Nanodiscs

There are several possible directions future studies of human rhodopsin could take. A recent innovation in membrane protein research is the nanodisc (*23*), which uses membrane scaffold proteins to form artificial membrane bicelles. Previous work with rhodopsin reconstituted in nanodiscs has shown that nanodisc preparations have the superior optical qualities of detergent solutions while preserving the kinetics seen in the native membrane (*24*). These preparations have proven invaluable for studying rhodopsin mutants or cone pigments, which are obtained in very low yields and could otherwise only be studied in detergent. Human rhodopsin reconstituted in nanodiscs would have the same advantage of enhanced optical quality. This would also allow a direct comparison between human and bovine rhodopsins without concern for differing membrane composition – any differences between human and bovine rhodopsin in nanodiscs could then only be from the protein.

3.2 Temperature and pH Dependence

Bovine rhodopsin has a well-characterized temperature- and pH-dependent equilibrium at its metarhodopsin I_{380} – metarhodopsin I_{480} branch point. This equilibrium exists in human rhodopsin as well, as can be partially seen in this study. However, the work here focused on human rhodopsin at pH 8.7 and 15°C, where all of the intermediates can be clearly seen, rather than covering the entire range of applicable temperatures and pH. A potential future investigation could examine the detailed temperature and pH dependencies on the equilibrium constants, analogous to the bovine studies done previously (*12*) (*16*). Human rhodopsin appears to follow the same general trends as bovine rhodopsin, but it is unknown how this holds over a wider range of conditions.

References

1. Rask-Andersen, M.; Almén, M. S.; Schiöth, H. B. Trends in the exploitation of novel drug targets. *Nature Reviews Drug Discovery* **2011,** No. 10, 579-590.
2. Nathans, J.; Hogness, D. S. Isolation and nucleotide sequence of the gene encoding human rhodopsin. *Proc. Natl. Acad. Sci. USA* **1982,** *81,* 4851-4855.
3. Palczewski, K.; Kumasaka, T.; Hori, T.; Behnke, C. A.; Motoshima, H.; Fox, B. A.; Trong, I. L.; Teller, D. C.; Okada, T.; Stenkamp, R. E.; Yamamoto, M.; Miyano, M. Crystal Structure of Rhodopsin: A G Protein-Coupled Receptor. *Science* **2000,** *289* (5480), 739-745.
4. Choe, H. W.; Kim, Y. J.; Park, J. H.; Morizumi, T.; Pai, E. F.; Krauss, N.; Hofmann, K. P.; Scheerer, P.; Ernst, O. P. Crystal structure of metarhodopsin II. *Nature* **2011,** *471* (7340), 651-655.
5. Li, J.; Edwards, P. C.; Burghammer, M.; Villa, C.; Schertler, G. F. Structure of bovine rhodopsin in a trigonal crystal form. *J Mol Biol* **2004,** *343* (5), 1409-1438.
6. Wald, G.; Durell, J.; George, R. C. C. S. The Light Reaction in the Bleaching of Rhodopsin. *Science* **1950,** *111* (2877), 179-181.
7. Yoshizawa, T.; Kito, Y.; Ishigami, M. Studies on the Metastable States in the Rhodopsin Cycle. *Biochimica et Biophysica Acta* **1960,** No. 43, 329-334.
8. Yoshizawa, T.; Wald, G. Pre-lumirhodopsin and the Bleaching of Visual Pigments. *Nature* **1963,** *197* (4874), 1279-1286.

9. Matthews, R. G.; Hubbard, R.; Brown, P. K.; Wald, G. Tautomeric Forms of Metarhodopsin. *Journal of General Physiology* **1963,** *47,* 215-239.

10. Hug, S. J.; Lewis, J. W.; Einterz, C. M.; Thorgeirsson, T. E.; Kliger, D. S. Nanosecond Photolysis of Rhodopsin: Evidence for a New, Blue-shifted Intermediate. *Biochemistry* **1990,** No. 29, 1475-1485.

11. Szundi, I.; Lewis, J. W.; Kliger, D. S. Two Intermediates Appear on the Lumirhodopsin Time Scale after Rhodopsin Photoexcitation. *Biochemistry* **2003,** *42,* 5091-5098.

12. Thorgeirsson, T. E.; Lewis, J. W.; Wallace-Williams, S. E.; Kliger, D. S. Effects of Temperature on Rhodopsin Photointermediates from Lumirhodopsin to Metarhodopsin II. *Biochemistry* **1993,** *32,* 13861-13872.

13. Lewis, J. W.; Kliger, D. S. Photointermediates of Visual Pigments. *Journal of Bioenergetics and Biomembranes* **1992,** *24* (2), 201-210.

14. Thomas, Y. G.; Szundi, I.; Lewis, J. W.; Kliger, D. S. Microsecond Time-Resolved Circular Dichroism of Rhodopsin Photointermediates. *Biochemistry* **2009,** *48,* 12283-12289.

15. Epps, J.; Lewis, J. W.; Szund, l.; Kliger, D. S. Lumi I -> Lumi II: The Last Detergent Independent Process in Rhodopsin Photoexcitation. *Photochemistry and Photobiology* **2006,** No. 82, 1436-1441.

16. Jäger, S.; Szundi, I.; Lewis, J. W.; Mah, T. L.; Kliger, D. S. Effects of pH on Rhodopsin Photointermediates from Lumirhodopsin to Metarhodopsin II.

Biochemistry **1998,** *37,* 6998-7005.

17. Szundi, I.; Mah, T. L.; Lewis, J. W.; Jäger, S.; Ernst, O. P.; Hofmann, K. P.; Kliger, D. S. Proton Transfer Reactions Linked to Rhodopsin Activation. *Biochemistry* **1998,** *37,* 14237-14244.
18. Lewis, J. W.; Kuijk, F. J. G. M. v.; Thorgeirsson, T. E.; Kliger, D. S. Photolysis Intermediates of Human Rhodopsin. *Biochemistry* **1991,** No. 30, 11372-11376.
19. Kuijk, F. J. G. M. v.; Lewis, J. W.; Buck, P.; Parker, K. R.; Kliger, D. S. Spectrophotometric Quantitation of Rhodopsin in the Human Retina. *Investigative Ophthalmology & Visual Science* **1991,** *32,* 1962-1967.
20. Thorgeirsson, T. E.; Lewis, J. W.; Wallace-Williams, S. E.; Kliger, D. S. Photolysis of Rhodopsin Results in Deprotonation of its Retinal Schiff's Base Prior to Formation of Metarhodopsin II. *Photochemistry and Photobiology* **1992,** *56* (6), 1135-1144.
21. Lewis, J. W.; Kliger, D. S. Absorption Spectroscopy in Studies of Visual Pigments: Spectral and Kinetic Characterization of Intermediates. *Methods in Enzymology* **2000,** *315,* 164-178.
22. Cone, R. A. Rotational Diffusion of Rhodopsin in the Visual Receptor Membrane. *Nature New Biology* **1972,** *236,* 39-43.
23. Bayburt, T. H.; Grinkova, Y. V.; Sligar, S. G. Self-Assembly of Discoidal Phospholipid Bilayer Nanoparticles with Membrane Scaffold Proteins. *Nano Letters* **2002,** *2* (8), 853-856.

24. Tsukamoto, H.; Szundi, I.; Lewis, J. W.; Farrens, D. L.; Kliger, D. S. Rhodopsin in Nanodiscs Has Native Membrane-like Photointermediates. *Biochemistry* **2011,** *50* (22), 5086-5091.